Geology and metallogenic signature of gold occurrences at Scheelite Dome, Tombstone gold belt, Yukon

John L. Mair
Centre for Strategic Mineral Deposits, University of Western Australia[1]

Craig J.R. Hart[2] ***Richard J. Goldfarb***[3] ***Mark O'Dea***[4] ***Stewart Harris***[5]

Mair, J.L., Hart, C.J.R, Goldfarb, R.J., O'Dea, M. and Harris, S., 2000. Geology and metallogenic signature of gold occurrences at Scheelite Dome, Tombstone gold belt, Yukon. *In:* Yukon Exploration and Geology 1999, D.S. Emond and L.H. Weston (eds.), Exploration and Geological Services Division, Yukon, Indian and Northern Affairs Canada, p. 165-176.

ABSTRACT

The study area is centred on the 91.2 ± 0.9 Ma Scheelite Dome quartz-monzonite stock of the Tombstone Plutonic Suite (TPS). This stock and associated dykes and sills intrude highly deformed metasedimentary strata of the Yusezyu Formation of the Neoproterozoic to Lower Cambrian Hyland Group. The emplacement of TPS intrusions post-dates regional greenschist-facies metamorphism and multiple phases of ductile deformation related to the Tombstone strain zone. Although the Scheelite Dome stock hosts auriferous, sheeted quartz veins, extensive soil geochemistry indicates that the bulk of the gold resource is hosted in the variably hornfelsed metasedimentary rocks immediately south of the stock. The associated gold-in-soil anomaly forms an east-trending corridor of anomalous gold values (>80 ppb) approximately 6 km long by 1.5 km wide, with a more weakly defined eastern continuation. Where metasedimentary bedrock is exposed in the corridor, gold is hosted in fault-vein arrays, and less commonly as disseminated grains and in replacement zones. The styles and distribution of mineralization are largely controlled by brittle structures; a phase of east-west shortening was largely coeval with gold mineralization.

R-mode factor analysis of multi-element geochemical data indicates two geochemically distinct metal suites within the area of the gold-in-soil anomaly at Scheelite Dome. The first suite, characterized by Au-Te-Bi ± W ± As, possesses the stronger gold association and is typical of intrusion-related gold occurrences elsewhere in the Tombstone gold belt. The second suite displays a metal association of Ag-Pb-Zn-Cd-Sb ± Cu ± Au, which is more characteristic of mid-Cretaceous Ag-Pb-Zn mineralization in the Keno Hill district, located approximately 60 km to the east-northeast. Field observations, combined with soil geochemistry, suggest that the different metal associations are paragenetically related. However, the possibility of two distinct hydrothermal events cannot yet be ruled out.

RÉSUMÉ

La région à l'étude est centrée sur le dôme Scheelite, un petit massif intrusif de monzonite quartzifère appartenant à la Série plutonique de Tombstone (SPT) et datant de 91,2 ± 0,9 Ma. Ce petit massif intrusif, et les dykes et filons-couches qui lui sont associés, s'introduisent dans les couches métasédimentaires intensément déformées de la Formation de Yusezyu, du Groupe de Hyland datant du Néoprotérozoïque au Cambrien. La mise en place des intrusions de la SPT est postérieure au métamorphisme du faciès des schistes verts dans la région et aux multiples phases de déformation ductile reliées à la zone de déformation de Tombstone. Bien que le petit massif intrusif du dôme Scheelite renferme des groupes de filons de quartz aurifère, de nombreuses analyses géochimiques des sols révèlent que la plus grande partie de la minéralisation en or se retrouve dans les roches métamorphisées à des degrés variables en cornéennes immédiatement au sud du massif. Les teneurs anomales en or (>80 ppb) du sol forment un corridor d'orientation est-ouest, long de 6 km et large de 1,5 km environ, avec un prolongement moins bien défini vers l'est. L'or se trouve dans des filons du type faille et, par endroits, sous formes de dissémination et de zones de substitution, là où les roches métasédimentaires affleurent à l'interieur de ce corridor. Les styles et la répartition de la minéralisation suggèrent un net contrôle par des structures cassantes généralement contemporaines de celle-ci et formées au cours d'un épisode de raccourcissement suivant l'axe est-ouest.

L'analyse factorielle mode-R de données géochimiques multi-élémentaires indique la présence de deux séries métalliques géochimiquement distinctes à l'intérieur de l'anomalie en or du sol au dôme Scheelite. La première, Au-Te-Bi ± W ± As, présente la plus intense association avec l'or et est caractéristique des manifestations aurifères reliées aux intrusions ailleurs dans la zone aurifère de Tombstone. La deuxième série, dans laquelle sont associés Ag-Pb-Zn-Cd-Sb ± Cu ± Au, est davantage caractéristique des minéralisations du Crétacé moyen du district de Keno Hill, situé à environ 60 km à l'est-nord-est. Les observations sur le terrain combinées aux analyses géochimiques du sol suggèrent que les différentes associations métalliques sont paragénétiquement reliées. La possibilité de deux événement hydrothermaux distincts ne peut cependant être écartée.

[1]*University of Western Australia, Department of Geology and Geophysics, Perth, 6907, Australia, jmair@geol.uwa.edu.au*

[2]*Yukon Geology Program, craig.hart@gov.yk.ca*

3United States Geological Survey, Denver Federal Center, Box 25046, MS 973, Denver, CO 80225, USA

[4]*Riftore Consulting Inc., 700-700 West Pender Street, Vancouver, British Columbia, Canada V6C 1G8*

[5]*Equity Engineering Ltd., 700-700 West Pender Street, Vancouver, British Columbia, Canada V6C 1G8*

INTRODUCTION

Scheelite Dome, located 27 km northwest of Mayo in central Yukon (Fig. 1), forms a topographic high at the headwaters of two actively mined placer gold-bearing creeks. The summit (1506 m) is underlain by the Scheelite Dome quartz-monzonite stock of the mid-Cretaceous Tombstone Plutonic Suite (TPS). Two other TPS stocks are present in the area: 1) the Morrison Creek stock, located approximately 6 km to the east of Scheelite Dome; and 2) the Minto Lake stock, located 6 km to the south of Scheelite Dome. All of the stocks were emplaced at approximately 92 Ma into highly deformed miogeoclinal metasedimentary rocks of the Yusezyu Formation of the Neoproterozoic to Lower Cambrian Hyland Group (Murphy, 1997). Placer gold has been mined from creeks draining Scheelite Dome for more than a century; however, it has only been in the last decade that the primary gold lodes in the area have been evaluated as possible economic targets.

The exploration history of the Scheelite Dome property is summarized by Hulstein et al. (1999). Extensive soil sampling was carried out by H6000 Holdings Ltd., Kennecott Canada Exploration Inc., La Teko Resources Ltd, and, most recently, current property owners Copper Ridge Explorations Inc. This has identified a 6- by 1.5-km, east-trending corridor of anomalously high gold concentrations, in an area underlain by metasedimentary rocks immediately south of the Scheelite Dome stock (Figs. 2 and 3). The large geochemical anomaly reflects an extensive hydrothermal system that deposited anomalous amounts of gold, tellurium, bismuth, tungsten, arsenic, and antimony.

Tungsten-bearing skarn mineralization is known to occur in calcic metasedimentary rocks immediately adjacent to the northern side of the Scheelite Dome stock (Fig. 2; Kuran et al., 1982). Gold is also hosted in sheeted quartz-K-feldspar veins within the stock, whereas in metasedimentary rocks to the south of the stock, gold occurs in fault veins, extension veins, replacement zones and as disseminated grains. Locally, felsic dykes cut auriferous quartz veins within the Scheelite Dome stock, indicating that mineralization occurred prior to the final phases of mid-Cretaceous magmatic activity. East-trending lamprophyre dykes within, and south of the stock, also cut auriferous quartz veins. These dykes are elsewhere considered

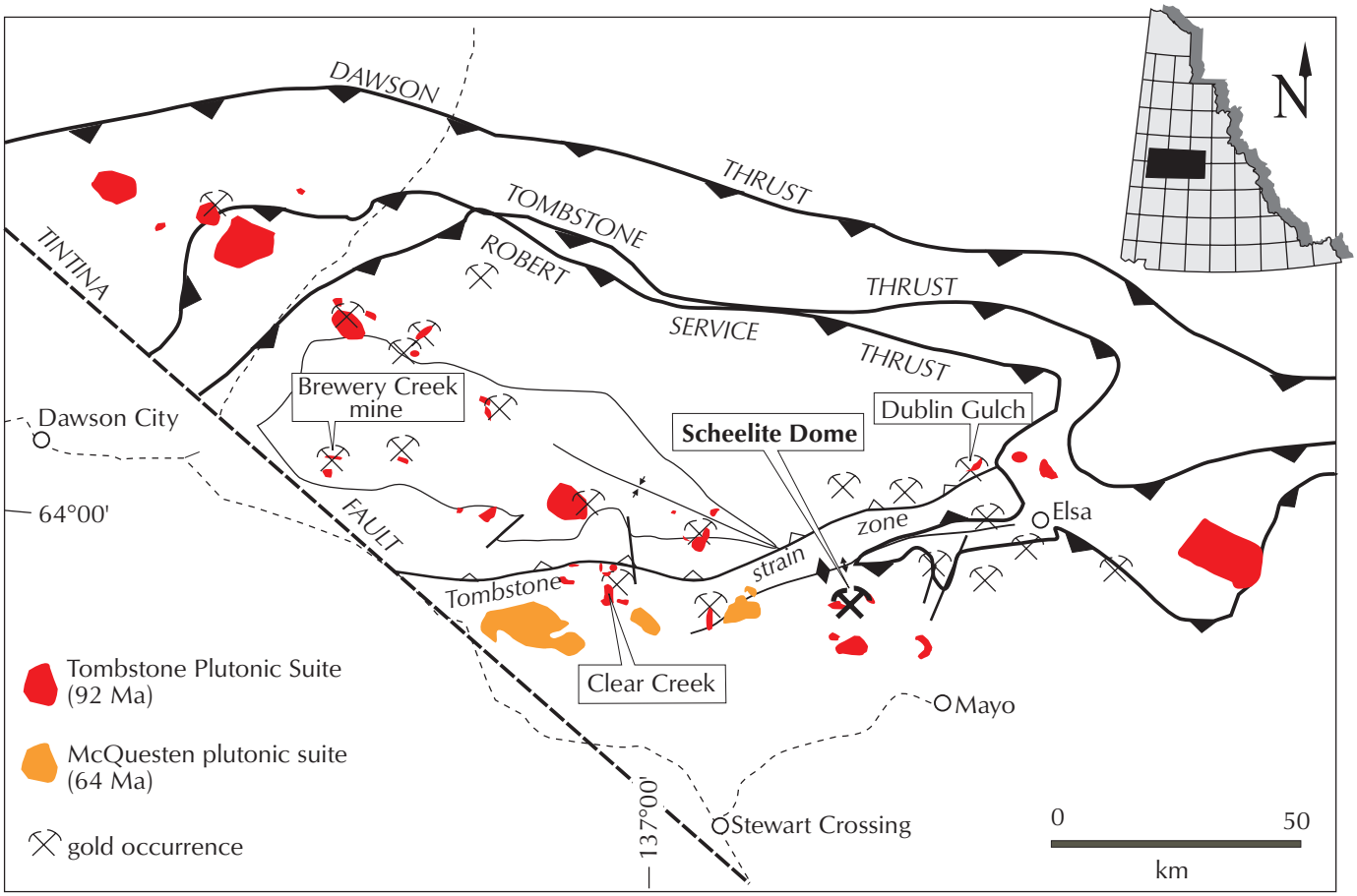

Figure 1. *Geological framework of the northern Selwyn Basin in west-central Yukon (modified after Murphy, 1997). The Scheelite Dome area is shown in Figure 2 and is located centrally within the Tombstone strain zone, near Mayo.*

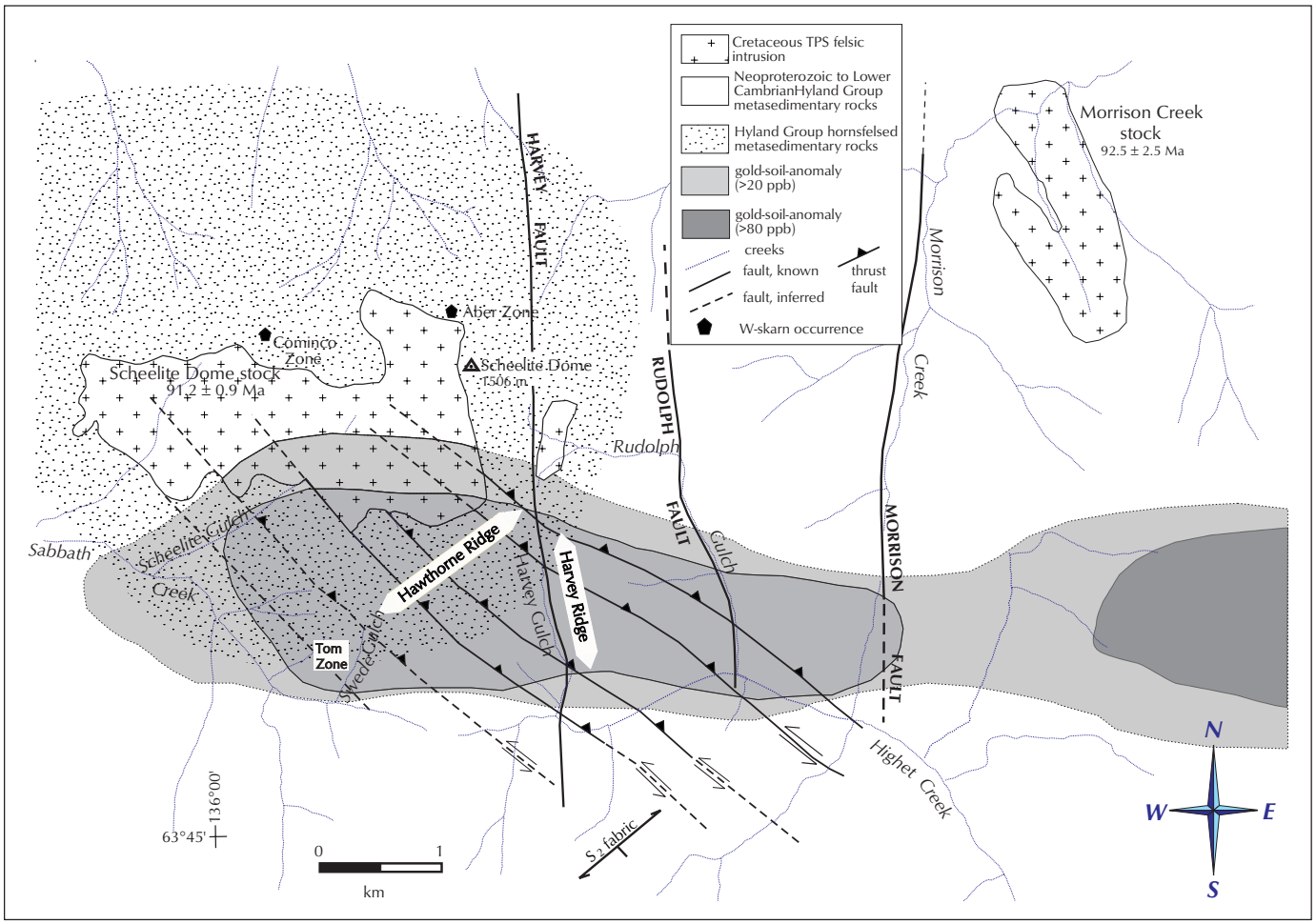

Figure 2. *Simplified geology of the Scheelite Dome area. The gold-in-soil anomaly indicates gold occurrences are concentrated within and beyond the thermal aureole, to the immediate south of the Scheelite Dome stock. Auriferous extension veins are best developed in psammitic rocks on Hawthorne and Harvey ridges; replacement-style gold occurrences are best developed at the Tom Zone; and disseminated gold-occurrences are best developed in psammites and phyllites between Harvey Ridge and Rudolph Gulch.*

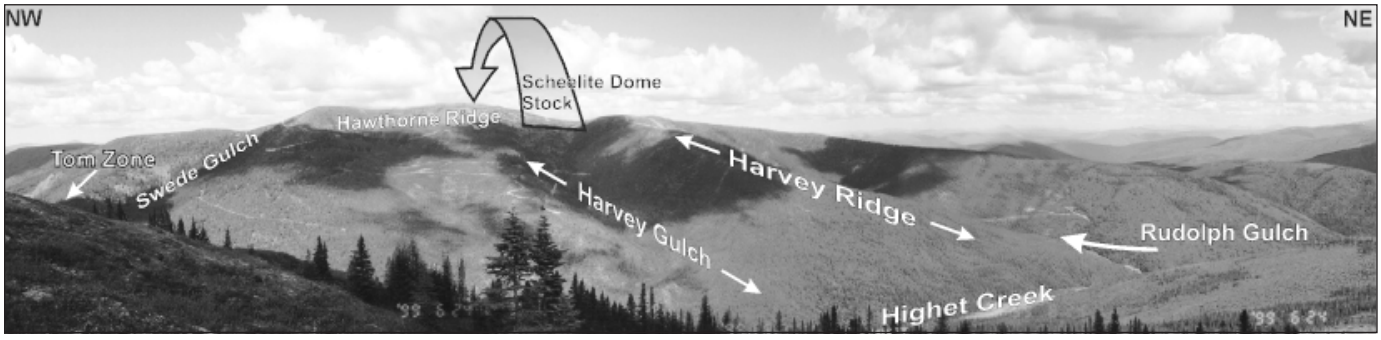

Figure 3. *View north toward Hawthorne and Harvey ridges. The Scheelite Dome stock weathers recessively, located behind Hawthorne Ridge (see Figure 2).*

to be related to TPS magmatism (Marsh et al., 1999; Gordey and Anderson, 1993). Hence, gold mineralization at Scheelite Dome bears a strong spatial and temporal relationship to the emplacement of TPS intrusions.

LOCAL GEOLOGY

LITHOSTRATIGRAPHY

The Scheelite Dome area is underlain by highly deformed miogeoclinal, metaclastic rocks of the Yusezyu Formation of the Neoproterozoic to earliest Paleozoic Hyland Group (Murphy, 1997). Psammitic and phyllitic rocks dominate the stratigraphy, with thin, metre-scale intercalations of calc-silicate rocks and carbonaceous siltstones. Psammitic rocks range from fine- to medium-grained, variably micaceous quartzites, to less commonly, quartzofeldspathic gritty psammites. Phyllitic rocks are composed of mainly chlorite and muscovite, with lesser biotite. The transition between phyllitic and psammitic rocks is commonly gradational due to extensive silica remobilization during high-strain deformation. Carbonaceous units are less than 1 m thick, and are characteristically dark and fine-grained. These units may contain disseminated, fine-grained syngenetic to diagenetic pyrite. Quartz-rich psammitic rocks commonly form ridges, in contrast to phyllitic rocks, which weather recessively.

Both the Scheelite Dome and Morrison Creek stocks are monzonitic, with biotite as the dominant mafic phase and minor hornblende. Both stocks are medium- to coarse-grained and are variably porphyritic with orthoclase phenocrysts. The surface expression of the Scheelite Dome stock is broadly east-trending, whereas the surface expression of the Morrison Creek stock is north-trending. Monzonitic sills and dykes, as much as a few metres in thickness, have intruded metasedimentary rocks surrounding the stocks. Aplite dykes cut the Scheelite Dome stock, and biotite-rich lamprophyre dykes cut both the Scheelite Dome stock and surrounding metasedimentary strata.

METAMORPHISM AND DEFORMATION

The metamorphic and deformational history of the Scheelite Dome area can be considered in two episodes: first, regional metamorphism and ductile deformation prior to the emplacement of the TPS; and, second, contact metamorphism and brittle deformation syn- to post-emplacement of the TPS.

Pre-TPS events

All sedimentary strata in the Scheelite Dome area have undergone regional mid-greenschist facies metamorphism, and been subjected to multiple phases of ductile deformation prior to the emplacement of TPS intrusions. Scheelite Dome is located centrally within the extensive, structurally complex, Tombstone strain zone, on the southern limb of the east-trending McQuesten Antiform (Murphy, 1997). Two main fabrics are developed in metasedimentary rocks in the area. The first, a pervasively transposed foliation (S_1), is subparallel to primary compositional layering. Micas formed during regional metamorphism are aligned with this fabric, clearly defining this foliation. The S_1 fabric has then been folded by northwest-verging, tight to isoclinal folds. The second significant fabric (S_2) forms the most prominent surface in the area, along which preferential weathering takes place. The S_2 fabric formed axial-planar to the northwest-verging, tight to isoclinal folds, strikes northeast, and dips moderately (30° to 50°) southeast (Fig. 4). In psammitic rocks, S_2 is commonly expressed as a spaced axial-planar cleavage, whereas in phyllitic rocks, S_2 is expressed as a pervasive foliation, sub-parallel to S_1. The variation in the expression of the S_2 fabric reflects different proportions

Figure 4. *The prominent S_2 fabric, formed axial-planar to tight folds of the S_1 regional metamorphic fabric, developed in psammite, Hawthorne Ridge (view toward the east).*

of strain accommodation by the rheologically contrasting phyllitic and psammitic rocks. Intersection lineations, defined by the intersection of the S_1 fabric with S_2 surfaces, commonly dip shallowly toward 070°. The S_2 fabric was later reactivated during high-strain, non co-axial deformation, as shear or 'C' surfaces. Shear bands are commonly well developed in phyllitic rocks, with 'S-C' shear-fabric relationships indicating north-northwest-directed movement. Other weakly developed ductile fabrics, which post-date the formation of S_2, are present locally and remain poorly understood. The S_2 fabric is also gently folded around north-trending axial planes. Such folds are rarely apparent at outcrop scale, but are recognized by variation in the orientation in S_2 at different outcrops. The gentle folds result in local variations in both the orientation of S_2, and the S_1-S_2 intersection lineation. The orientation of gentle folds infers a phase of east-west shortening, which post-dates ductile shearing.

Syn- to post-TPS events

The stocks in the Scheelite Dome area, as with many intrusions of the TPS, are surrounded by extensive and well developed contact metamorphic aureoles. These are characterized by the development of metamorphic silicate minerals and pyrrhotite, which overprint the pre-intrusion ductile fabrics (Murphy, 1997). Within a few hundred metres of the Scheelite Dome stock, metasedimentary strata exhibit partial fabric destruction due to recrystallization of quartz. Andalusite is well developed in phyllitic rocks as far as 1.5 km from the stock; however, beyond 1 km, biotite development is more ubiquitous, characterizing the outer hornfels zone. Aeromagnetic data indicate that the pyrrhotite development around the Scheelite Dome stock is relatively weak, particularly in comparison to pyrrhotite development around the Minto Lake stock, located 6 km to the south. This is likely a reflection of a greater proportion of authigenic-pyrite-bearing rocks (favoured for pyrrhotite development during contact metamorphism), such as phyllites and carbonaceous siltstones, in close proximity to the Minto Lake stock, whereas the Scheelite Dome stock intrudes a part of the miogeoclinal sequence characterized by a greater proportion of psammitic rocks.

Two generations of brittle faults, which postdate earlier ductile deformation, formed during TSP emplacement. The first generation strikes north and dips subvertically. The second generation strikes northwest, and dips moderately to steeply toward the northeast. Immediately adjacent to the north-trending Rudolph fault (Fig. 2), the S_2 fabric is drawn into alignment with the fault, in a manner indicating sinistral displacement. The same exposure of the fault is cut by east-trending mineralized quartz veins, confirming that formation of the north-trending faults pre-dated the mineralizing event. In contrast, mineralized quartz veins are locally drawn into the north-trending Harvey fault in such a manner as to indicate post-mineralization dextral displacement. North-striking faults form topographic and geophysical lineaments, and may, in part, have influenced the morphology of the Scheelite Dome stock, and to a greater degree, the north-trending Morrison Creek stock. Northwest-trending brittle faults display evidence for oblique-slip displacement, and clearly offset the Scheelite Dome stock. Offset along northwest-trending faults, as indicated by aeromagnetic data, clearly suggests sinistral displacement. However, in plan view, offset of the Scheelite Dome stock by northwest-trending faults appears dextral. This conflict can be explained by the shallowly south-dipping contact of the Scheelite Dome stock being offset by a component of reverse movement, raising hanging-wall blocks and resulting in apparent dextral offset in plan. A prominent set of east-striking tension fractures, which dip moderately to the north, are best developed in psammitic rocks across the ridges immediately to the south of the Scheelite Dome stock. Both northwest-striking faults and east-striking tension fractures host gold mineralization. North-trending faults locally contain massive milky quartz veins, but do not host gold mineralization. East-striking tension fractures also host post-mineralization lamprophyre dykes. There is no evidence of structural disruption immediately adjacent to Scheelite Dome, and there is only minor warping of the prominent S_2 fabric. Small TPS intrusions in the area occur as both sills concordant to the S_2 fabric, and as dykes exploiting the east-trending fractures, discordant to the S_2 fabric.

GOLD MINERALIZATION

The Scheelite Dome area features many of the styles of gold mineralization typical of the Tombstone gold belt (Poulsen et al., 1997; Hart et al., 2000), including sheeted quartz veins within the Scheelite Dome stock, as well as fault-vein arrays, disseminated gold grains, and replacement bodies in the surrounding metasedimentary rocks (*cf.* Hulstein et al., 1999). Extensive soil sampling across the property has identified an east-trending gold-in-soil anomaly (>80 ppb Au), which is approximately 6- by 1.5-km-wide, and with a 2-km-long continuation of the anomaly to the east (Fig. 2). Throughout the gold-in-soil anomaly, arsenic concentrations are mostly above 100 ppm, and antimony concentrations are commonly above 5 ppm. The positioning of the anomaly indicates that the bulk of the gold resource occurs within, and beyond the thermal aureole, immediately south of the Scheelite Dome stock.

Gold in the Scheelite Dome stock is hosted in predominantly east-trending, variably dipping, sheeted quartz-K-feldspar veins typical of intrusion-hosted gold mineralization elsewhere in the Tombstone gold belt (Poulsen et al. 1997). Arsenopyrite is the dominant sulphide mineral, comprising between 0.5 to 2% by volume of the veins. Alteration adjacent to veins is extremely subtle, with weak chloritization of feldspars. Late felsic dykes locally cut the sheeted veins within the stock, suggesting a late-magmatic relative timing for vein emplacement.

Surrounding the Scheelite Dome stock, extension veins (Fig. 5a) generally range from 2 mm to 20 cm in width. The quartz veins contain variable amounts of carbonate, and 1 to 10% by volume sulphide minerals, which include arsenopyrite, stibnite, and lesser pyrite. Extension veins are surrounded by sericite alteration selvages, which extend laterally for up to 5 times the thickness of the vein. Fault veins feature characteristic crack-seal textures (Fig. 5b) and polyphase brecciation. They occur sporadically along northwest-trending faults, suggesting certain areas of faults were dilational and favoured fluid pathways. The best exposed fault vein, the Hawthorne vein, features an early quartz generation, followed by a quartz-arsenopyrite stage, and then a late massive-sulphide stage of predominately stibnite. Veins are commonly surrounded by sericitic alteration haloes of variable width and intensity. Disseminated gold mineralization (Fig. 5c) occurs locally within psammites and phyllites. It is associated with areas of pervasive sericitization, variable degrees of silicification, and disseminated arsenopyrite, lesser pyrite, and rare bismuthinite. Such zones commonly display evidence of elevated structural permeability in the form of randomly oriented fracture networks. Replacement-style gold mineralization (Fig. 5d) is restricted to variably calcareous rocks, with folioform replacement dominated by pyrrhotite, with lesser arsenopyrite and rare chalcopyrite. Notably, this style of mineralization occurs in more distal settings from the Scheelite Dome stock than tungsten-bearing skarn mineralization, concentrated in calcareous rocks immediately north of the stock (Fig. 2).

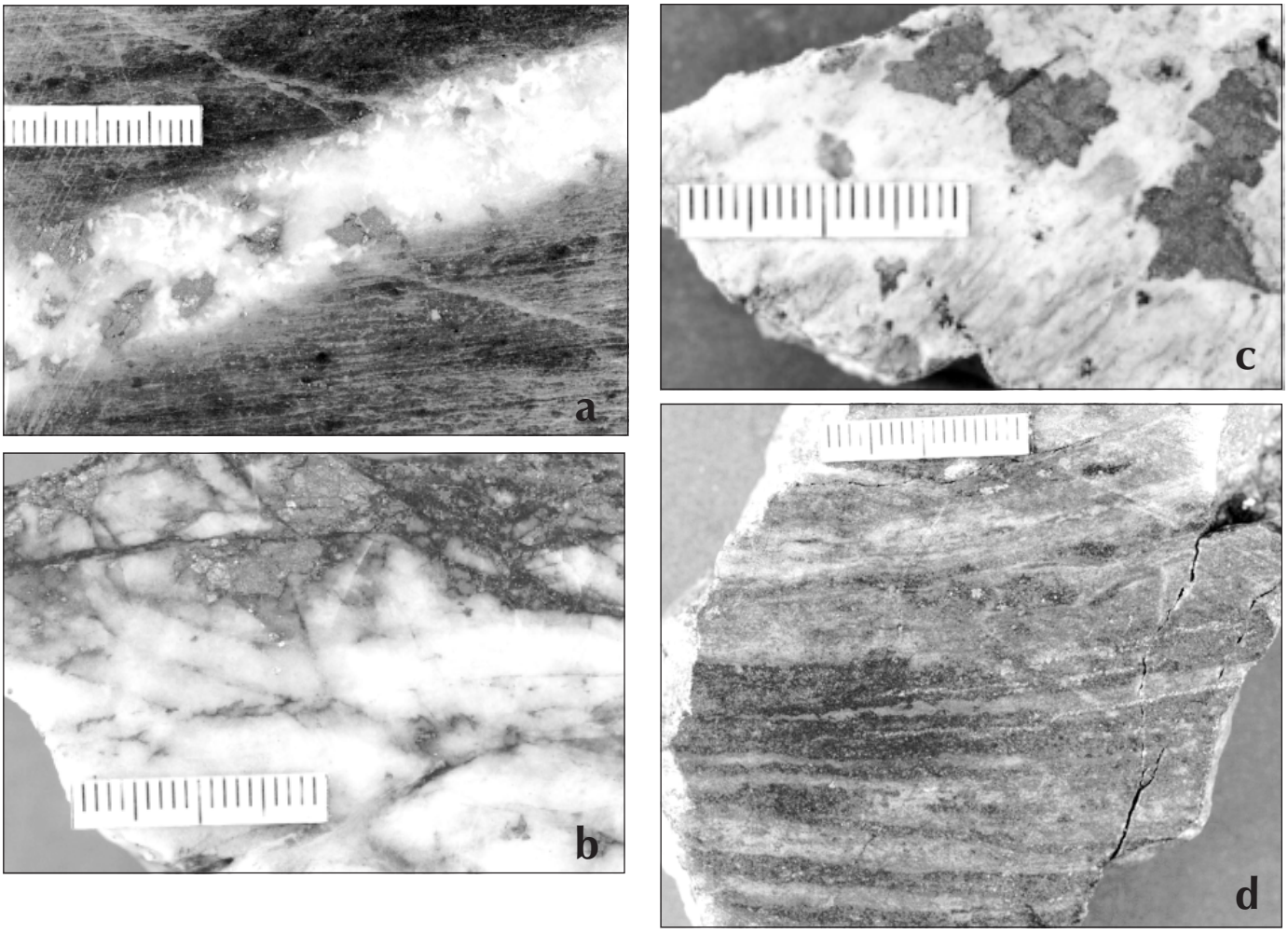

Figure 5. *Styles of gold mineralization at Scheelite Dome: a) quartz-arsenopyrite extension veins; b) typical fault-vein material displaying crack seal textures (stibnite is concentrated along fractures in the quartz-arsenopyrite assemblage); c) disseminated arsenopyrite in sericitized quartz-phyllite; and d) folioform replacement of calc-silicate rock by pyrrhotite, lesser arsenopyrite, and minor chalcopyrite.*

STRUCTURAL CONTROL

The distribution of gold mineralization at Scheelite Dome is largely controlled by the interaction of northwest-trending, northeast-dipping faults, and east-trending, north-dipping tension fractures. Both structural elements contain similar gold-bearing hydrothermal assemblages. The east-striking fractures are responsible for the east-trend of the gold-in-soil anomaly; however, lateral constrains, to the north and south, along the corridor of hydrothermal activity, remain undetermined. Crack-seal textures in the northwest-trending fault veins indicate multiple failure events and fluid pulses during the life span of the hydrothermal system. East-trending extension veins (Fig. 6) are locally cut at low angles by similarly oriented, extension veins, suggesting that tension fractures formed synchronous with hydrothermal activity. Although east-trending tension fractures are well developed in both the footwalls and hanging walls of northwest-trending faults, the majority of veins are hosted by fractures in the hanging walls (Fig. 7). Quartz crystals in extension veins exhibit growth normal to vein margins, indicating pure extension. Slickenlines on exposed northwest-trending faults indicate oblique-slip displacement, such that the inferred extension direction corresponds to that for east-trending extension veins (a north-oriented, south-plunging, minimum compressive stress). Such structural relationships infer a phase of east-west shortening, and inclined north extension (Fig. 7) during the gold-forming events. This correlates with an interpreted phase of east-west shortening during the formation of mineralized brittle faults at Clear Creek, located approximately 50 km to the west (Stevens, this volume). Lamprophyre dykes, which post-date gold mineralization at Scheelite Dome, also exploit the same east-trending fractures, suggesting that the far-field stress regime was maintained subsequent to the hydrothermal activity.

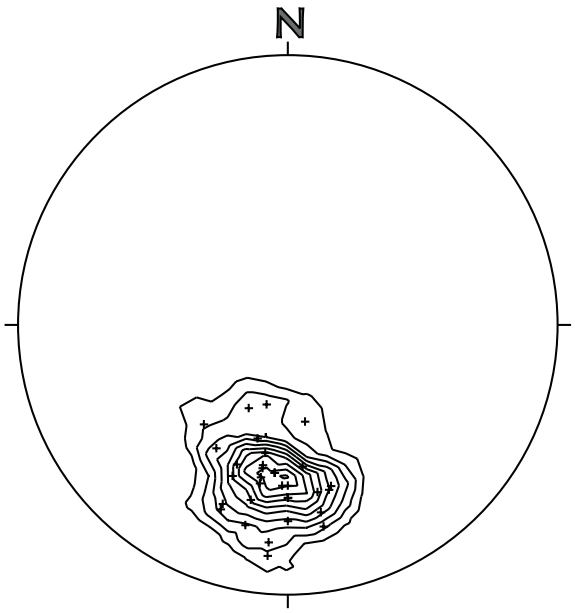

Figure 6. *Equal area, lower hemisphere projection, poles to auriferous-quartz extension veins from Hawthorne and Harvey ridges, and Rudolph Gulch.*

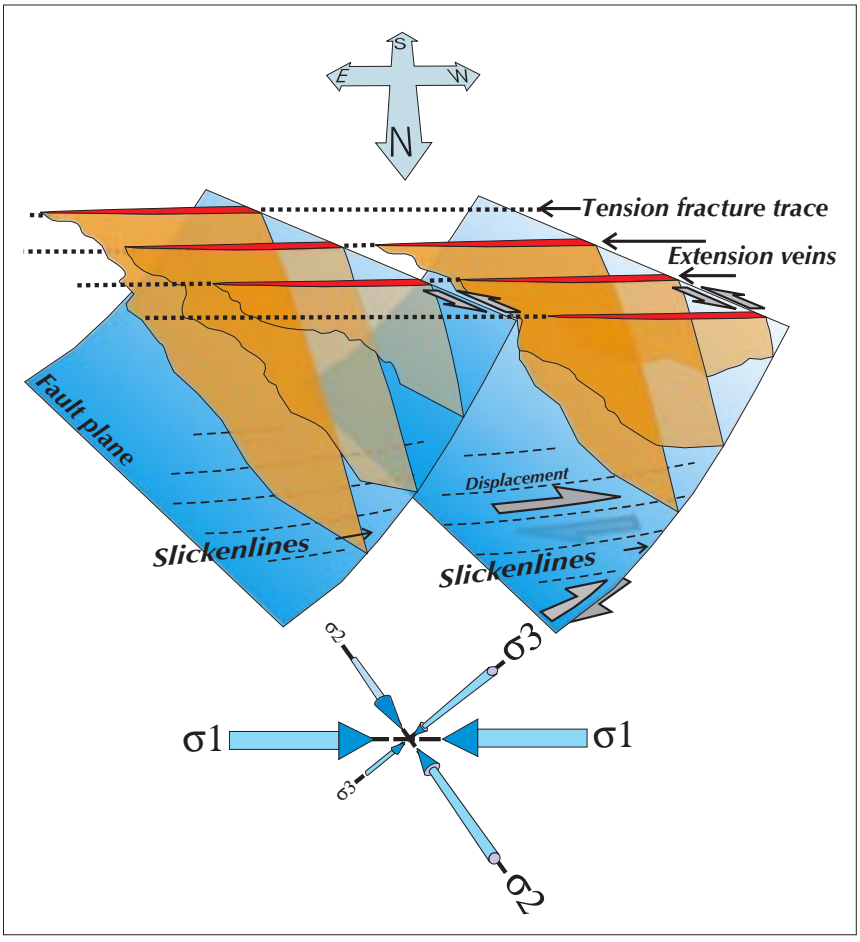

Figure 7. *Schematic depiction of the key structures controlling mineralization and the inferred orientation of the far-field stress regime at the time (view toward the south). Note, extension veins are best developed in the hanging walls of northwest-trending faults.*

METAL GEOCHEMISTRY OF THE SCHEELITE DOME GOLD OCCURRENCES

Grab samples and drill core samples, of hydrothermally altered wallrock or metalliferous vein material, were collected throughout the extent of the main gold-in-soil anomaly, spanning from the Tom Zone in the west, to east of Rudolph Gulch (Fig. 2). Of the 102 samples submitted for analyses, the majority were hydrothermally altered metasedimentary rocks, within and beyond the extent of the hornfels zone surrounding the Scheelite Dome stock. All styles of mineralization (as discussed above) were sampled. Analyses were performed by Acme Analytical Laboratories Ltd., Vancouver, B.C. (Table 1). Gold concentrations were determined to a lower detection limit of 5 ppb by standard fire assay with atomic absorption (AA) finish. Concentrations of 31 other major, minor, and trace elements in the 102 samples were determined by inductively coupled plasma-atomic emission spectroscopy (ICP-AES) analysis. Samples were also analyzed for tellurium by AA methods.

Arsenic concentrations are >1000 ppm in 70% of the samples since arsenopyrite was, by far, the most widely visible sulphide phase observed during sampling of metalliferous outcrops in the field. However, samples containing high arsenic levels do not consistently show high gold values (r = 0.57). Antimony concentrations are also consistently elevated, with 40% of the samples containing >100 ppm. All mineralization styles are characterized by a broad range of gold concentrations. Although only 18 samples of disseminated and replacement mineralization styles were analyzed, they include more than half of all the samples with greater than 4 ppm Au. This suggests any high-grade targets that are eventually delineated during future resource estimation are likely to be within zones characterized by these mineralization styles. Of the nine samples containing >10 ppm Au, most also contain >300 ppm W and >50 ppm Bi. Samples with Sb concentrations >1000 ppm, consistently feature Pb concentrations >100 ppm.

FACTOR ANALYSES

R-mode factor analysis, using Varimax rotation of log-transformed data, was used to identify the main elemental associations within the geochemical data set. This information was used in an attempt to characterize the metallogenic signature(s) of gold mineralization. Factor analysis enables a large, multivariate data set to be explained by a small number of factors, which identify the dominant associations between variables (i.e., the elements). The calculated factor loadings may be interpreted similarly to correlation coefficients, with highest absolute loadings onto each factor defining a group of variables that are strongly inter-correlated within the data set. Factor analyses were performed using Stat View™ 512+. Results of the factor analysis are presented in Table 2. In order to carry out the factor analysis, elemental concentrations below the limit of detection were replaced with values 0.7 times the lower detection limit. Highly censored elements (containing a large proportion of 'less than' values), including uranium and thallium, were eliminated from the analysis. Because geochemical data distributions are typically log-normal, a log transformation of all data was performed prior to factor analysis. A six-factor model was used to explain approximately 77% of the total variance within the Scheelite Dome lithogeochemical database. Additional factors were deemed statistically insignificant because they were characterized by Eigen values <1.0 and thus explained less of the data variance than the single elements themselves.

The calculated second and fourth factors define the precious metal associations at Scheelite Dome. The strongest loading for gold is onto factor 4, which also contains high loadings for tellurium and bismuth, and, to a lesser degree, Ag, As, Fe and W. Examination of factor scores (i.e., the relative correlation of each sample with that factor association) indicates that all styles of mineralization may be characterized by the factor 4 metal suite and there is no obvious spatial restriction to the suite. This factor suggests that bismuth- and tellurium-bearing mineral phases are most consistently associated with gold in the Scheelite Dome occurrences. The high loadings for arsenic and tungsten reflect the common presence of arsenopyrite and scheelite; silver is likely enriched with gold as electrum. The high loading for iron particularly reflects the high pyrrhotite content of replacement-style samples (such as samples 3 and 4 from the Tom Zone, and sample 92 from Rudolph Gulch, Table 1), which have notably high scores onto factor 4.

Factor 2 defines a second, significant gold-bearing association. It is characterized by a strong base metal association, with high factor loadings for Ag, Pb, Zn, Cd, Sb, and, to a lesser degree, Cu, Au, and As. Samples that score highly onto factor 2 include those of paragenetically late, massive sulphide mineralization (predominately stibnite) from within fault veins and quartz-stibnite-arsenopyrite extension veins (e.g., samples 19 and 64, Table 1). The factor loading onto Au may be exaggerated, due to fault-vein samples incorporating different paragenetic stages, including an earlier Au-rich phase characterized by the metal association in factor 4 (Fig. 5b). It is possible that this association represents a greater metal contribution leached from the metasedimentary rocks, when compared to the association of factor 4. It is also interesting to note that Marsh et al. (1999) determined the same two gold-related associations at Clear Creek, which further suggests that this is a regional feature inherent to the hydrothermal systems.

Factor 1 contains high loadings for Fe, Na, Ca, Mg, Al, Ti, Sr, V, Ni, Co, and Mn. This association is representative of analyzed samples that simply contained a large proportion of metasedimentary rock, as most of the elements in the

Table 1. *Lithogeochemical data for mineralized samples collected throughout the extent of the gold-in-soil anomaly at Scheelite Dome (see Figure 2 for location of anomalous zones). Most elemental concentrations are ppm; Au is in ppb; Fe, Ca and Mg are in percent. Mineralization abbreviations: rep. = replacement; dis. = disseminated; f.v. = fault vein; e.v. = extension vein.*

Sample no.	Description	Mineralization style	Mo	Cu	Pb	Zn	Ag	Ni	Co	Mn	Fe	As	Cd	Sb	Bi	V	Ca	La	Cr	Mg	Ba	W	Te	Au
Tom Zone																								
1	calc-silicate rock	rep.	31	17	2.1	11	0.21	22	6	240	0.59	100	0.14	2.1	5	23	4.28	14	17	0.39	63	10	0.18	256
2	gritty psammite	dis.	3	14	11	4	1.4	4	1	58	0.63	3406	0.14	42	7	2	0.08	14	19	0.03	27	9	0.4	543
3	calc-silicate rock	rep.	5	767	4	10	5.4	83	71	739	17.73	3589	0.14	3	301	18	5.29	16	14	0.51	20	323	8.6	10032
4	calc-silicate rock	rep.	5	1450	2.1	18	8	66	113	966	15.92	6354	0.14	10	510	29	5.88	17	17	0.8	35	529	18.28	18041
5	calcareous psammite	dis.	3	111	21	52	11.9	48	102	2283	7.09	18369	0.3	3929	2292	45	11.61	11	18	2.81	47	693	52.48	57873
Hawthorne Ridge																								
6	early quartz phase	f.v.	5	11	6	1	0.8	2	1	29	0.33	535	0.14	910	2.1	1	0.007	1	29	0.007	2	3	0.014	32
7	quartz-arsenopyrite vein	e.v.	5	4	4	4	0.5	3	1	60	0.51	510	0.14	66	3	1	0.01	4	30	0.01	30	5	0.02	54
8	quartz-arsenopyrite vein	e.v.	1	4	6	4	0.7	3	1	71	0.61	819	0.14	44	2.1	1	0.01	4	25	0.01	58	8	0.03	87
9	quartz-arsenopyrite vein	e.v.	1	7	52	10	1.3	12	3	189	0.64	1019	2.4	89	5	3	0.04	15	22	0.02	30	64	0.03	104
10	psammite with quartz-arsenopyrite vein	e.v.	1	17	6	9	0.5	5	2	59	0.83	614	0.14	10	5	3	0.01	12	24	0.06	70	5	0.08	123
11	psammite with quartz-arsenopyrite vein	e.v.	5	13	37	14	1.9	8	2	104	0.94	1453	0.14	19	6	5	0.03	16	27	0.07	95	4	0.43	136
12	psammite with quartz-arsenopyrite vein	e.v.	0.7	15	6	17	0.5	15	8	382	1.43	2910	0.14	14	3	3	0.04	18	22	0.04	133	8	0.13	179
13	psammite with quartz-arsenopyrite vein	e.v.	3	26	21	31	0.4	8	3	175	2.96	3767	1.1	41	6	14	0.04	40	38	0.37	160	5	0.12	237
14	quartz-arsenopyrite vein	e.v.	5	4	9	1	1.2	2	0.7	45	0.58	3632	0.14	20	2.1	1	0.01	2	32	0.007	97	4	0.24	256
15	quartz-arsenopyrite vein	e.v.	21	27	11	21	1.1	8	3	73	2.24	7725	0.3	129	2.1	4	0.03	17	31	0.06	192	4	0.22	300
16	phyllite with quartz-arsenopyrite-stibnite vein	e.v.	2	10	67	7	10.4	3	1	36	0.99	2139	0.14	647	6	2	0.01	14	20	0.01	49	7	0.21	385
17	psammite with quartz-arsenopyrite vein	e.v.	5	18	27	9	2.1	2	1	59	2.59	17945	0.14	133	4	3	0.01	19	24	0.01	118	3	0.1	451
18	quartz-arsenopyrite, stibnite vein	f.v.	5	29	2358	15	37.5	1	1	56	1.14	9312	3.4	2565	11	1	0.01	6	31	0.007	383	5	0.7	517
19	massive sulphide	f.v.	1	312	260	366	274.7	0.7	3	28	1.03	507	12	50937	11	1	0.01	2	21	0.01	4	4	0.03	808
20	altered quartz-phyllite	dis.	1	36	59	14	5.9	1	1	56	3.39	14589	0.6	182	5	3	0.01	35	14	0.02	104	2	0.17	1033
21	quartz-arsenopyrite vein	e.v.	1	24	767	182	9.5	4	2	88	2.79	46447	13.7	525	6	2	0.02	10	24	0.01	255	8	0.24	1264
22	psammite with quartz-arsenopyrite vein	e.v.	3	31	323	42	18	17	3	160	2.99	11758	0.7	232	41	15	0.03	20	40	0.32	63	4	2.92	1381
23	brecciated vein-quartz	f.v.	7	159	28	21	1.2	7	3	42	4.6	1492	1.6	17	6	2	0.01	4	26	0.01	12	4	0.61	1539
24	quartz-arsenopyrite, stibnite vein	f.v.	1	75	7414	92	61.3	1	1	111	3.69	85306	35.8	3396	16	3	0.04	13	22	0.01	266	4	0.33	1720
25	quartz-arsenopyrite, stibnite vein	f.v.	2	48	61	4	16	1	4	31	1.45	15514	0.5	11945	4	1	0.007	3	26	0.007	3	6	1.71	1792
26	phyllite with quartz-arsenopyrite vein	e.v.	1	23	1868	111	17.7	4	2	102	3.69	85420	15	1131	8	5	0.03	14	18	0.03	184	4	0.28	2122
27	altered quartz-phyllite with vein	e.v.	4	19	827	49	15.2	2	1	91	4.02	84231	5.5	567	11	2	0.03	9	23	0.01	355	2	0.4	2286
28	quartz-arsenopyrite vein	e.v.	10	7	36	5	1.9	4	2	70	0.58	1519	0.2	64	142	2	0.01	4	34	0.01	8	5	5.09	3670
29	quartz-arsenopyrite, stibnite vein	f.v.	9	158	4691	420	90.2	0.7	1	43	1.7	17616	227.7	4755	15	1	0.01	1	32	0.007	5	5	0.67	4712
30	quartz-arsenopyrite, stibnite vein	f.v.	6	33	803	8	32.1	0.7	1	45	1.52	16842	3.7	2966	62	0.7	0.01	1	33	0.007	30	5	2.19	17583
Harvey Ridge/Harvey Gulch																								
31	quartz breccia	f.v.	1	93	9	48	0.21	17	6	130	6.72	1712	0.14	35	2.1	4	0.01	18	15	0.01	24	5	0.02	5
32	quartz breccia	f.v.	4	29	6	60	0.8	26	7	181	6.83	4375	0.14	236	5	3	0.04	23	19	0.01	155	3	0.05	25
33	quartz vein	e.v.	1	4	3	1	0.3	3	1	41	0.38	50	0.14	4	3	0.7	0.007	2	17	0.01	6	20	0.09	46
34	psammite with quartz-arsenopyrite vein	e.v.	1	11	9	20	0.3	7	2	90	1.2	1012	0.14	26	2.1	3	0.01	18	14	0.02	87	5	0.24	47
35	psammite with quartz-arsenopyrite vein	e.v.	5	6	4	6	0.5	3	2	153	0.71	695	0.14	10	2.1	2	0.01	10	23	0.01	81	5	0.11	47
36	psammite with quartz-arsenopyrite vein	e.v.	4	5	5	8	0.4	4	2	316	0.75	629	0.14	12	2.1	2	0.01	13	20	0.01	47	4	0.08	57
37	psammite with quartz-arsenopyrite vein	e.v.	3	6	3	4	0.21	2	1	154	0.52	463	0.14	8	2.1	1	0.01	10	26	0.01	33	5	0.11	61
38	psammite with quartz-arsenopyrite vein	e.v.	1	8	9	15	0.5	6	2	189	1.03	1204	0.14	11	2.1	2	0.01	15	17	0.02	67	7	0.19	65
39	psammite with quartz-arsenopyrite vein	e.v.	2	25	10	19	0.7	14	5	422	1.43	2732	0.14	21	5	4	0.96	15	17	0.25	32	5	0.45	72
40	phyllite with quartz veinlets	e.v.	1	3	4	5	0.9	2	1	43	0.45	210	0.14	88	2.1	2	0.007	17	17	0.01	28	4	0.03	72
41	psammite with quartz-arsenopyrite vein	e.v.	2	25	8	8	0.6	11	4	236	1.15	344	0.14	13	3	2	0.63	11	17	0.18	21	5	0.14	91
42	quartz-arsenopyrite vein	e.v.	1	20	7	9	0.8	4	1	69	0.79	1297	0.14	14	3	3	0.01	12	18	0.03	42	13	0.29	111
43	psammite with quartz-arsenopyrite vein	e.v.	4	18	21	16	1.4	12	3	114	1.37	1068	0.14	16	2.1	3	0.01	17	22	0.01	39	6	0.14	122
44	quartz-arsenopyrite vein	e.v.	3	5	116	8	2.9	7	1	203	0.93	2612	0.8	60	3	2	0.01	11	21	0.01	73	8	0.48	132
45	psammite with quartz-arsenopyrite vein	e.v.	2	15	23	30	1.2	17	8	558	2.02	870	0.14	42	2.1	2	1.06	9	15	0.35	115	4	0.16	190
46	psammite with quartz-arsenopyrite-stibnite vein	e.v.	4	23	3174	39	17.9	6	1	51	1.14	3837	3.3	393	2.1	2	0.007	16	17	0.02	26	6	0.23	194
47	psammite with quartz-arsenopyrite vein	e.v.	3	10	8	15	0.21	12	3	329	1.39	2883	0.14	21	2.1	2	0.51	13	19	0.16	23	7	0.21	217
48	psammite with quartz-arsenopyrite-stibnite vein	e.v.	4	11	2836	17	15.3	6	0.7	47	0.83	3567	2.6	320	2.1	1	0.007	6	15	0.01	19	8	0.26	222
49	psammite with quartz-arsenopyrite vein	e.v.	2	9	20	12	0.6	10	2	129	1.15	2226	0.14	33	2.1	2	0.02	15	16	0.02	157	6	0.23	229
50	phyllite with quartz-arsenopyrite vein	e.v.	4	3	10	4	0.7	3	1	43	1	5814	0.2	9	4	2	0.01	10	27	0.01	243	4	1.45	240
51	phyllite with quartz-arsenopyrite vein	e.v.	3	12	6	29	0.21	14	5	559	2.22	504	0.14	17	2.1	8	0.36	13	28	0.35	29	4	0.06	241
52	psammite with quartz-arsenopyrite veins	e.v.	3	30	10	11	1.4	13	5	233	1.78	10379	0.14	43	5	2	0.41	11	19	0.15	26	5	2.49	275
53	psammite with quartz-arsenopyrite vein	e.v.	1	5	7	5	0.9	3	1	37	0.64	2270	0.14	9	2.1	1	0.01	14	14	0.01	44	5	1.15	308
54	psammite with quartz-arsenopyrite vein	e.v.	1	33	11	37	0.7	20	11	117	2.14	1888	0.14	10	4	7	0.03	42	20	0.15	82	2	0.33	326
55	altered psammite with disseminated arsenopyrite	dis.	1	9	7	8	0.8	3	1	40	0.79	4669	0.14	10	2.1	2	0.02	14	14	0.01	22	5	0.42	386
56	quartz-stibnite vein	e.v.	1	70	32	185	18.4	0.7	1	55	0.74	179	13.8	19084	2.1	1	0.02	2	20	0.01	11	1.4	0.03	458
57	phyllite with quartz-arsenopyrite vein	e.v.	3	27	16	13	0.9	25	9	383	1.76	5820	0.2	236	5	4	0.19	22	17	0.1	63	9	0.41	506
58	phyllite with quartz-arsenopyrite vein	e.v.	8	18	7	7	0.3	2	1	52	2.22	6300	0.4	14	4	4	0.01	33	15	0.02	123	5	0.82	647
59	psammite with quartz-arsenopyrite vein	e.v.	3	10	74	5	1.6	6	1	62	1.1	7522	0.14	31	4	2	0.01	11	21	0.01	18	6	0.94	667
60	psammite with quartz-arsenopyrite vein	e.v.	125	23	12	61	0.6	28	11	430	2.7	1051	0.14	31	14	3	0.39	19	17	0.58	46	7	0.77	795
61	psammite with quartz-arsenopyrite vein	e.v.	3	21	8	31	0.4	20	8	280	2.51	12223	0.3	28	3	4	0.24	20	20	0.23	43	5	3.16	802
62	phyllite with quartz-arsenopyrite vein	e.v.	4	20	26	25	0.9	16	6	288	1.66	942	0.14	35	11	9	0.78	11	29	0.35	49	8	0.52	803
63	gritty psammite with quartz-arsenopyrite vein	e.v.	3	53	21	8	2.1	13	7	219	2.2	18806	0.14	75	12	2	0.47	10	18	0.13	27	7	6.03	847
64	massive sulphide	f.v.	1	141	2.1	13	16.7	0.7	2	17	0.33	44	0.9	19026	105	1	0.007	1	4	0.01	1	1.4	0.03	859
65	quartz-arsenopyrite vein	e.v.	3	12	290	2	130.4	7	1	52	0.64	2807	1.1	187	4	1	0.007	2	20	0.007	107	9	0.08	1057
66	psammite with quartz-arsenopyrite vein	e.v.	4	39	23	23	1.6	13	7	479	1.75	5203	0.3	41	3	2	0.56	12	21	0.21	28	5	1.02	1132
67	phyllite with quartz-arsenopyrite vein	e.v.	2	42	23	60	0.5	58	22	349	3.85	17137	0.14	25	6	16	0.13	21	26	0.69	93	5	2.25	1429

continued...

Table 1. *continued (most elemental concentrations are ppm; Au is in ppb; Fe, Ca and Mg are in percent. Mineralization abbreviations: rep. = replacement; dis. = disseminated; f.v. = fault vein; e.v. = extension vein.)*

Sample no.	Description	Mineralization style	Mo	Cu	Pb	Zn	Ag	Ni	Co	Mn	Fe	As	Cd	Sb	Bi	V	Ca	La	Cr	Mg	Ba	W	Te	Au
68	quartz breccia	f.v. ?	2	12	181	3	61.9	7	1	66	1.28	11974	0.5	70	3	1	0.02	8	14	0.01	218	7	0.24	1468
69	altered psammite	dis.	5	17	330	10	11.2	5	1	59	1.85	17449	0.3	205	4	1	0.007	9	22	0.01	89	7	0.4	1633
70	psammite with quartz-arsenopyrite-veins	e.v.	5	18	24	23	0.9	10	3	721	2.79	13008	0.2	1442	4	2	1.61	11	29	0.52	35	8	3.77	1728
71	altered monzonite dyke	dis.	4	204	21	26	1.5	25	15	935	4.43	10004	0.5	309	18	8	1.96	50	11	0.47	86	3	0.47	1735
72	quartz-stibnite vein	f.v.	1	247	55	92	16.1	10	8	277	1.62	982	1.8	19236	2.1	1	0.34	2	15	0.17	8	3	0.02	1899
73	phyllite with quartz-arsenopyrite vein	e.v.	6	25	29	3	2.4	32	8	125	0.8	3472	0.14	28	24	2	0.53	22	20	0.02	38	6	1.62	2196
74	phyllite with quartz-arsenopyrite-stibnite vein	e.v.	5	29	4247	340	54.8	5	1	55	0.93	5995	91.8	3524	6	1	0.007	2	26	0.007	132	4	0.19	2548
75	phyllite with quartz-arsenopyrite-stibnite vein	e.v.	2	32	2570	248	25.1	7	2	62	2.92	8490	56	1304	8	6	0.05	32	11	0.02	99	19	0.63	2865
76	phyllite with quartz-arsenopyrite vein	e.v.	4	8	3	14	0.4	7	3	120	1.59	1841	0.14	6	2.1	3	0.03	13	20	0.03	17	4	0.36	4068
77	altered monzonite dyke	dis.	4	296	50	47	3.4	38	15	752	4.49	14344	1	68	29	9	0.97	45	16	0.35	43	3	0.74	4171
78	phyllite with quartz-stibnite-arsenopyrite vein	e.v.	3	78	25281	50	232.5	0.7	1	53	1.11	2310	56.4	25482	39	2	0.01	7	18	0.03	39	1.4	0.08	11233
79	psammite with quartz vein	e.v.	4	5	22	5	3.3	4	1	58	0.58	438	0.14	42	540	2	0.02	6	23	0.01	29	324	15.06	12307
80	psammite with disseminated arsenopyrite	dis.	2	22	83	11	12.5	16	29	262	4.77	51242	1.5	258	145	3	1.56	12	15	0.33	30	658	5.78	34419
81	phyllite with quartz-arsenopyrite vein	e.v.	2	46	125	82	10.6	66	26	723	5.53	35867	0.8	84	27	9	0.74	17	14	0.86	59	1.4	3.92	59575
Rudolph Gulch																								
82	phyllite with quartz-arsenopyrite vein	e.v.	2	7	6	19	0.3	10	1	97	0.91	3679	0.2	20	2.1	2	0.02	13	19	0.02	48	7	0.16	59
83	calc-silicate rock with disseminated arsenopyrite	dis.	2	131	5	20	0.3	102	50	497	4.77	30543	0.3	30	6	64	3	10	64	1.17	33	1.4	0.22	77
84	psammite crosscut by quartz vein	e.v.	3	30	5	19	0.8	11	3	105	0.96	1097	0.14	86	4	3	0.01	19	17	0.02	62	4	0.11	93
85	psammite with quartz-arsenopyrite-stibnite vein	e.v.	3	17	246	32	4.3	14	3	121	1.42	1596	0.14	480	4	8	0.01	13	26	0.14	65	5	0.12	96
86	psammite with quartz-arsenopyrite vein	e.v.	4	14	10	14	0.7	9	3	151	1.16	4378	0.9	28	2.1	3	0.03	21	21	0.02	538	6	0.27	101
87	psammite with quartz-arsenopyrite vein	e.v.	3	11	65	16	1.4	11	2	105	0.91	3692	0.3	440	3	3	0.02	16	18	0.02	33	12	0.27	120
88	psammite with quartz-arsenopyrite vein	e.v.	3	8	18	13	0.6	16	4	369	1.13	3993	0.14	437	2.1	3	0.01	14	23	0.02	176	6	0.24	133
89	quartz-arsenopyrite vein	f.v.?	3	12	16	10	0.7	9	2	127	0.74	2023	0.4	20	2.1	1	0.03	4	23	0.02	7	9	0.03	159
90	quartz-arsenopyrite, stibnite vein	f.v.?	5	26	253	39	90.3	8	2	65	0.84	6079	5.4	310	3	1	0.01	4	25	0.007	21	32	0.13	213
91	psammite with quartz-arsenopyrite vein	e.v.	1	21	5	20	0.5	11	4	152	1.73	4457	0.14	7	8	4	0.04	53	12	0.04	57	4	0.23	436
92	calc-silicate rock (partially replaced)	rep.	2	405	7	38	0.3	41	22	389	5.47	26731	0.2	49	28	26	1.77	22	37	1.04	35	5	0.68	461
93	psammite with quartz-arsenopyrite veinlets	e.v.	4	8	235	30	4.8	7	1	70	0.88	4871	2.4	113	3	1	0.05	10	19	0.02	8	6	0.03	685
94	quartz-arsenopyrite vein	e.v.	6	8	601	8	7.5	8	1	78	1.47	13627	2.6	219	11	1	0.01	1	30	0.007	5	12	0.16	1247
95	quartz-arseonpyrite-stibnite vein	e.v.	4	40	1352	8	12.4	6	0.7	77	2.43	23850	0.8	749	36	2	0.02	3	20	0.007	34	8	2.26	1404
96	massive sulphide	f.v.	1	244	270	407	134.8	5	4	90	0.45	254	45.1	19798	28	1	0.27	2	7	0.01	3	1.4	0.04	1611
97	quartz-arsenopyrite-stibnite vein	f.v.?	2	1865	21040	173	288.3	0.7	1	47	3.23	14883	64.1	20431	24	1	0.06	3	14	0.01	13	3	0.11	2131
98	quartz-arsenopyrite-stibnite vein	e.v.	2	39	2632	24	52.7	6	1	70	1.04	8914	6.5	2844	17	1	0.02	1	26	0.007	3	10	0.1	2542
99	calc-silicate rock (partially replaced)	rep.	1	1839	16	16	2.8	44	25	358	20.09	6046	0.14	37	362	22	1.26	28	29	0.58	15	155	4.05	3041
100	psammite with quartz-arsenopyrite vein	e.v.	4	38	6	37	2.6	14	5	99	2.64	1816	0.14	30	7	6	0.01	17	25	0.14	100	18	0.45	3401
101	psammite with disseminated arsenopyrite	dis.	3	55	31	14	3.1	4	2	71	3.06	32211	1.4	47	16	2	0.02	12	17	0.03	64	34	0.55	3448
102	quartz-arsenopyrite vein	e.v.	5	12	847	7	15.4	9	2	132	1.15	7589	0.3	815	61	3	0.02	4	24	0.03	40	478	1	16523

Table 2*. Six-factor model of R-mode factor analysis of lithogeochemical data presented in Table 1. Factors 2 and 4 describe the metallogenic associations, whereas factors 1, 3 ,5 and 6 describe lithological associations. Positive numbers indicate the degree of positive correlation. The strongest gold association occurs in Factor 4.*

Element	Factor 1	Factor 2	Factor 3	Factor 4	Factor 5	Factor 6
Mo	0.153	-0.162	-0.15	0.141	0.468	-0.494
Cu	0.516	0.571	-0.061	0.235	-0.197	0.319
Pb	-0.268	0.792	0.075	0.242	0.187	-0.099
Zn	0.352	0.773	0.207	-0.187	-0.072	-0.02
Ag	-0.24	0.797	-0.132	0.39	-0.095	0.017
Ni	0.804	-0.287	0.165	0.054	0.044	-0.06
Co	0.882	-0.026	0.077	0.174	-0.137	0.079
Mn	0.864	-0.138	0.168	0.014	-0.022	-0.246
Fe	0.621	0.262	0.409	0.355	0.079	0.145
As	0.032	0.376	0.53	0.552	0.132	-0.097
Th	0.357	-0.368	0.753	0.041	-0.21	0.06
Sr	0.674	0.173	0.359	0.248	-0.089	-0.156
Cd	-0.199	0.894	-0.058	0.071	0.029	-0.03
Sb	-0.134	0.847	-0.125	0.062	-0.088	-0.002
Bi	0.346	0.234	-0.189	0.795	-0.094	0.17
V	0.795	-0.118	0.295	0.092	0.209	0.316

Element	Factor 1	Factor 2	Factor 3	Factor 4	Factor 5	Factor 6
Ca	0.884	-0.036	-0.027	0.168	-0.159	-0.187
P	0.504	-0.011	0.611	0.145	0.217	0.192
La	0.384	-0.305	0.797	0.006	-0.141	0.134
Cr	0.095	-0.08	-0.053	-0.061	0.875	0.006
Mg	0.92	-0.093	0.14	0.043	0.014	-0.018
Ba	0.029	-0.129	0.748	0.026	0.287	-0.11
Ti	0.636	-0.033	0.023	-0.066	0.402	0.529
B	-0.477	0.108	0.464	-0.028	-0.121	-0.047
Al	0.742	-0.159	0.491	0.028	0.055	0.29
Na	0.71	-0.081	0.093	0.141	0.062	0.429
K	0.418	-0.133	0.742	-0.15	-0.101	0.022
W	0.212	-0.309	-0.348	0.552	0.059	-0.082
Te	0.322	-0.048	0.217	0.799	0.023	-0.058
Hg	0.038	0.275	0.175	-0.022	0.483	0.022
Au	0.169	0.453	0.038	0.751	-0.138	-0.045
Cumulative %	33.7	51.3	62.1	67.7	73.6	77

association form common silicate and carbonate mineral phases. Factor 3 is defined by high loadings for Th, P, La, Ba, and K, and, to a lesser extent, for Fe, B and Al. Samples with high scores onto factor 3 are the most intensely sericitically altered phyllitic and psammitic rocks, although they may or may not be enriched in gold. Factor 5 contains high loadings for Mo, Cr, and Hg, and most likely explain the variance in the data due to a few samples with a high component of black shale protolith. Factor 6 is also interpreted to reflect minor lithogeochemical variations among a few samples.

DISCUSSION OF THE FACTOR ANALYSIS

Results of the factor analysis indicate that many of the gold-rich lodes at Scheelite Dome are characterized by a metallogenic signature of Au-Te-Bi ± W, As ± Ag, Fe. This signature is broadly consistent with that for other gold occurrences within the Tombstone gold belt, including Clear Creek (Marsh et al., 1999), Fort Knox (Bakke, 1995), and Dublin Gulch (Smit et al., 1996). Elements such as Te, Bi, and W are often assumed to be associated with magmatic hydrothermal systems (Sillitoe and Thompson, 1998). If correct, then this element association may define hydrothermal fluids exsolved from the Scheelite Dome crystallizing magma or a leaching of the stock by hydrothermal fluids from any source subsequent to crystallization.

The strong base metal association in factor 2, which is also associated with elevated gold levels at Scheelite Dome, as well as at Clear Creek (Marsh et al., 1999), is somewhat characteristic of the mineralization in the Keno Hill district (approximately 60 km to the east-northeast). Lynch (1986) recognized a regional zonation in metals and associated hydrothermal assemblages over a 25-km-long, east-trending corridor of mid-Cretaceous hydrothermal activity in the Keno Hill district. He speculated that the eastern-most mineral occurrences, dominated by pyrrhotite, arsenopyrite, and gold, were, on a district scale, most proximal to the primary fluid source. They were hypothesized to represent the deeper metallogenic expression of the widespread, zoned hydrothermal system. The extensively-mined central Keno Hill and Galena Hill areas near Elsa (Fig. 1) contained a large Ag-Pb-Zn resource, which was thought to perhaps have reflected a shallower, cooler part to the hydrothermal system (Lynch, 1986).

At Scheelite Dome, it remains to be determined whether a more telescoped, but geochemically similar, hydrothermal system is also defined by an early Au-W-Bi-Te-As fluid and a later Au-Ag-Pb-Zn-Sb fluid pulse. Initial evaluation of our data from Scheelite Dome suggests no apparent spatial zonation of metals within the aerial extent of the hydrothermal system. However, samples with highest scores onto factor 2 tend to be characterized by late-stage massive sulphide mineralization in fault veins. Therefore, it is interpreted that enrichment of base metals may represent a later paragenetic stage within the evolution of the hydrothermal system. Additional study is required before we can determine whether the metals in both stages likely have been derived from the same sources.

SUMMARY

Scheelite Dome hosts multiple styles of gold mineralization, and tungsten- and tin-bearing skarn occurrences. Extensive soil and rock sampling have identified an east-trending geochemical anomaly greater than 6 km long, indicative of an extensive hydrothermal system. Field evidence indicates that gold mineralization bears a temporal and spatial relationship to the Scheelite Dome quartz monzonite stock of the TPS, although most significant occurrences are distal to the stock, within and near the thermal aureole. The distribution of gold mineralization at Scheelite Dome is mainly controlled by northwest-trending brittle faults, and east-trending tension fractures, formed during a phase of east-west shortening that was coeval with the mineralizing event. Styles of gold mineralization in metasedimentary rocks include extension veins, fault veins, replacement zones, and disseminated zones. The diversity of mineralization styles outside the stock reflects the chemical and rheological heterogeneity of the metasedimentary strata. Within the Scheelite Dome stock, gold is only hosted in sheeted quartz-K-feldspar veins.

R-mode factor analyses of the log-transformed lithogeochemical data for mineralized grab and drill core samples indicates two precious metal associations within the extent of the soil geochemical anomaly at Scheelite Dome. The most consistent gold association occurs with Bi-Te ± As, W, which is broadly consistent with granitoid-hosted gold occurrences elsewhere in the Tombstone gold belt. The second precious metal association features a strong Ag-Pb-Zn-Sb-Cd ± Cu, As association, which is more characteristic of Ag-Pb-Zn mineralization in the nearby Keno Hill district. Field evidence, combined with soil and grab sample geochemistry, indicate that there is no apparent spatial zonation of metals within the extent of the soil geochemical anomaly at Scheelite Dome. However, rock samples which feature the Ag-Pb-Zn-Sb-Cd ± Cu, As, Au association, are typically paragenetically late, suggesting that the two precious metal associations may be related to different paragenetic stages in the evolution of the hydrothermal system.

ACKNOWLEDGEMENTS

Thanks to Copper Ridge Explorations Ltd. for access to the Scheelite Dome property and all available data. Julian Stephens, Erin Marsh, Mark Lindsay and Don Murphy are thanked for constructive discussions throughout the field season. The Society of Economic Geologists is acknowledged for financial support. A special thanks to Leyla Weston and Diane Emond for having the patience to wait diligently for this manuscipt. Finally, the Pointer Brothers are acknowledged for their quality tunes during field breaks in Dawson.

REFERENCES

Bakke, A.A., 1995. The Fort Knox "porphyry" gold deposit – Structurally controlled stockwork and shear quartz vein, sulphide-poor mineralisation hosted by Late Cretaceous pluton, east-central Alaska. *In*: Porphyry Deposits of the Northwestern Cordillera of North America, T.A. Shoeter (ed.), Canadian Institute of Mining and Metallurgy, Special Volume 46, p. 795-802.

Gordey, S.P. and Anderson, R.G., 1993. Evolution of the northern Cordilleran miogeocline, Nahanni map area (105I), Yukon and Northwest Territories. Geological Survey of Canada, Memoir 428.

Hart, C.J.R., Baker, T. and Burke, M., 2000. New exploration concepts for country-rock hosted intrusion-related gold systems: Tintina gold belt in Yukon. Cordilleran Round Up volume, in press.

Hulstein, R., Zuran, R., Carlson G.G. and Fields, M., 1999. The Scheelite Dome gold project, central Yukon. *In*: Yukon Exploration and Geology 1998, C.F. Roots and D.S. Emond (eds.), Exploration and Geological Services Division, Yukon, Indian and Northern Affairs Canada, p. 185-196.

Kuran, V.M., Godwin, C.I. and Armstrong, R.L., 1982. Geology and geochronometry of the Scheelite Dome tungsten-bearing skarn property, Yukon Territory. Canadian Institute of Mining and Metallurgy, vol. 75, p. 137-142.

Lynch, G., 1986. Mineral zoning in the Keno Hill silver-lead mining district, Yukon. *In*: Yukon Geology, Volume 1, J.A. Morin and D.S. Emond (eds.), Exploration and Geological Services Division, Yukon, Indian and Northern Affairs Canada, p. 89-97.

Marsh, E.E., Hart, C.J.R., Goldfarb, R.J. and Allen, T.L., 1999. Geology and geochemistry of the Clear Creek gold occurrences, Tombstone gold belt, central Yukon Territory. *In*: Yukon Exploration and Geology 1998, C.F. Roots and D.S. Emond (eds.), Exploration and Geological Services Division, Yukon, Indian and Northern Affairs Canada, p. 185-196.

Murphy, D.C., 1997. Geology of the McQuesten River region, northern McQuesten and Mayo map areas, Yukon Territory (115P/14,15,16; 105M/13,14). Exploration and Geological Services Division, Yukon, Indian and Northern Affairs Canada, Bulletin 6, 122 p.

Poulsen, K.H., Mortensen, J.K. and Murphy, D.C., 1997. Styles of intrusion-related gold mineralization in the Dawson-Mayo area, Yukon Territory. *In*: Current Research 1997-A, Geological Survey of Canada, p. 1-10.

Sillitoe, R.H. and Thompson, J.F.H., 1998. Intrusion-related vein gold deposits: Types, tectono-magmatic settings and difficulties of distinction from orogenic gold deposits. Resource Geology, vol. 48, p. 237-250.

Smit, H., Sieb, M. and Swanson, C., 1996. Summary information on the Dublin Gulch project, Yukon Territory. *In*: Yukon Exploration and Geology 1995. Exploration and Geological Services Division, Yukon, Indian and Northern Affairs Canada, p. 33-36.

Stephens, J.R., Oliver, N.H.S., Baker, T. and Hart, C.J.R., 2000 (this volume). Structural evolution and controls on gold mineralization at Clear Creek, Yukon. Yukon Exploration and Geology 1999, D.S. Emond and L.H. Weston (eds.), Exploration and Geological Services Division, Yukon, Indian and Northern Affairs Canada, p. 151-163.